

Electronic Supplementary Information (ESI)

Solvent-triggered relaxative spin state switching of [Fe(HB(pz)₃)₂] in closed nano-confinement of NH₂-MIL- 101(Al)[†]

Tian Zhao,^a Ishtvan Boldog,^{*,a} Vojislav Spasojevic,^b Aurelian Rotaru^c, Yann Garcia^d and Christoph Janiak^{*,a}

^a Institut für Anorganische Chemie und Strukturchemie, Universität Düsseldorf, Universitätsstr. 1, D-40225 Düsseldorf, Germany. *E-mails: tianzhao696@yahoo.com.hk, ishtvan.boldog@gmail.com, janiak@uni-duesseldorf.de

^b Belgrade University, Institute for Nuclear Sciences, P. O. Box 522, 11001 Beograd, Serbia. E-mail: vojas@vin.bg.ac.rs

^c Dept. of Electrical Engineering and Computer Science, Ștefan cel Mare University, University Street 13, 720229 Suceava, Romania. E-mail: aurelian.rotaru@usm.ro

^d Institute of Condensed Matter and Nanosciences, Molecules, Solids and Reactivity (IMCN/MOST), Université catholique de Louvain, Place L. Pasteur 1, 1348 Louvain-la-Neuve, Belgium. E-mail: yann.garcia@uclouvain.be

Molecular structure of $[\text{Fe}(\text{HB}(\text{pz})_3)_2]$

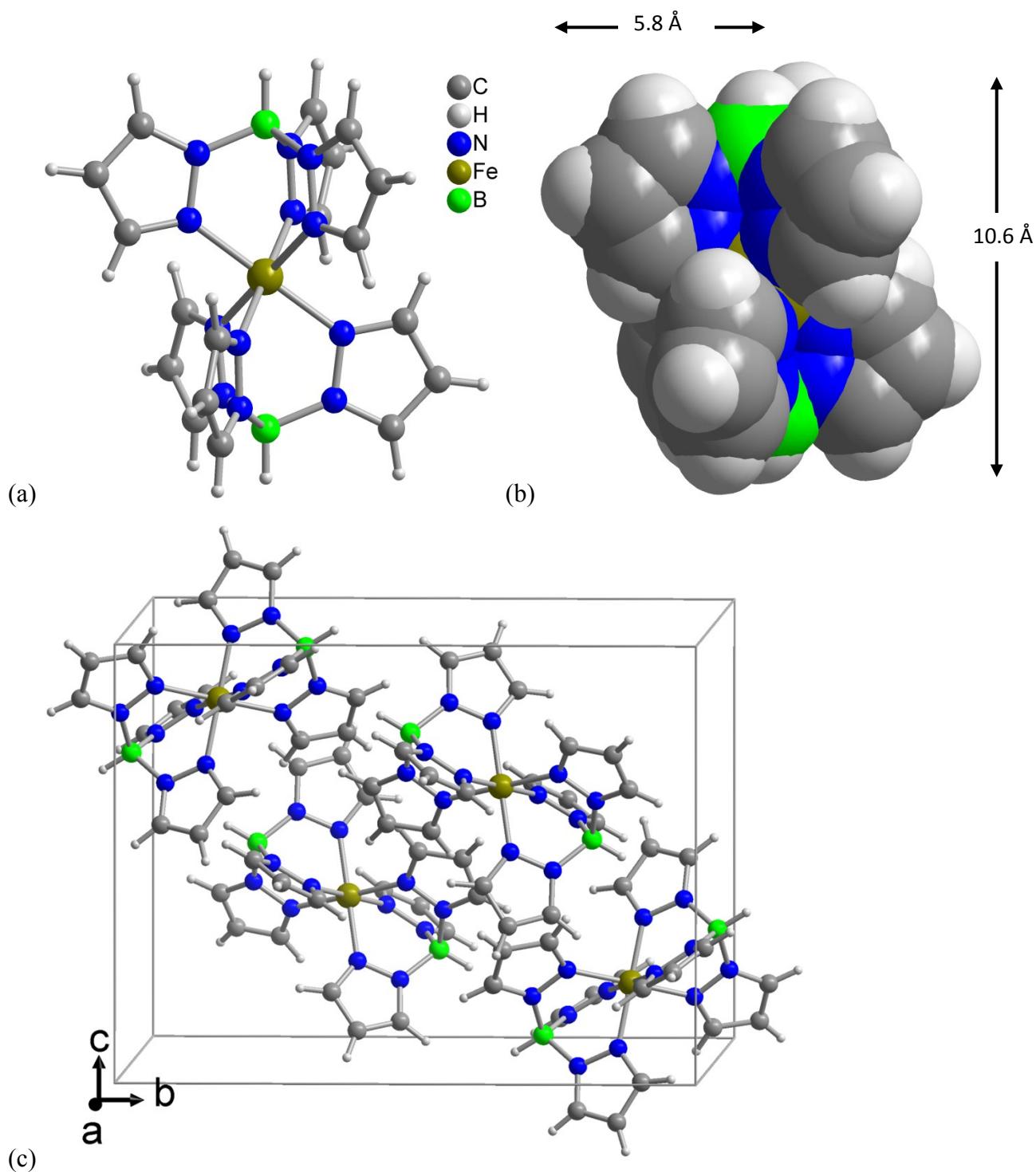


Fig. S1 Single-crystal X-ray structure of $[\text{Fe}(\text{HB}(\text{pz})_3)_2]$ (Refcode HPZBFE03);¹ (a) ball-and-stick presentation, (b) space-filling presentation of single molecule, (c) unit-cell packing.

Estimation of the molecular volume of $[\text{Fe}(\text{HB}(\text{pz})_3)_2]$: the shape of the molecule is approximated by a cylinder with a height of 10.6 Å and a radius of 5.8 Å (Fig. S1b). The height is estimated as the H(B)⋯(B)H distance of 8.16 Å and twice of the van-der-Waals radius of a hydrogen atom 1.2 Å, which add up to ~10.6 Å.

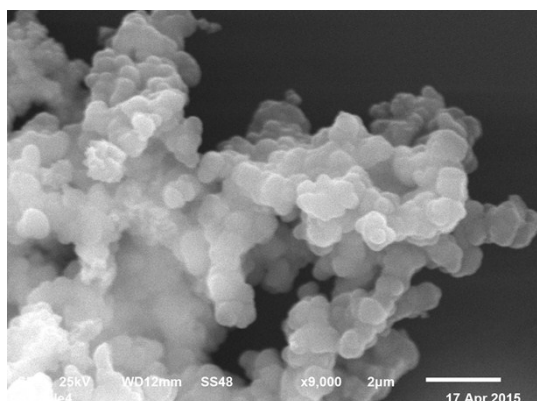
The radius is estimated from the H(4-C)⋯ B distance of 4.60 Å with the vdW radius of the hydrogen atom, 1.2 Å, added to give 5.8 Å. The volume of the model cylinder is $\pi r^2 h = 3.14 \times (5.8)^2 \times 10.6 \text{ Å}^3 = 357 \text{ Å}^3$.

On the other hand the volume of space associated with a single molecule, as derived from one of the reported single-crystal XRD structures of $[\text{Fe}(\text{HB}(\text{pz})_3)_2]$ with unit cell volume of 2157.85(78) Å³ and $Z = 4$, is $2158 / 4 = 540 \text{ Å}^3$.

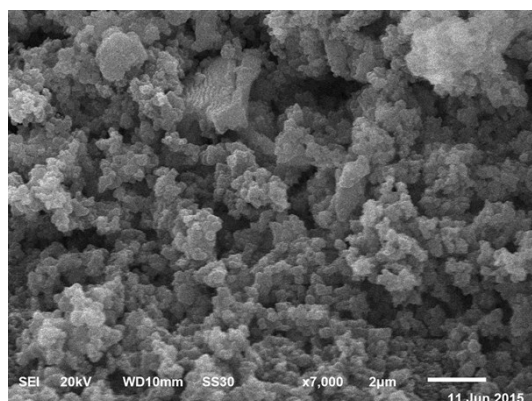
The ratio of the two values, $357 / 540 = 0.66$ is in effect the estimated packing coefficient and it is within the range of 0.65-0.77 characteristic for the majority of molecular crystals,² which corroborates the molecular volume estimation by using the simple cylinder model.

Scanning electron microscopy

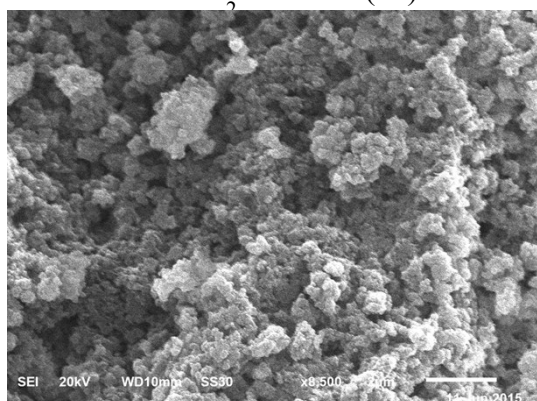
Scanning electron microscopy (SEM) images (Fig. S2) show the morphology of NH₂-MIL-101(Al) with irregular particles, which is in a good agreement with the reported literature.³ The morphology of S@M composites is similar to the bulk NH₂-MIL-101(Al). This supports the assumption that the iron containing species should be located inside the pores of NH₂-MIL-101(Al).



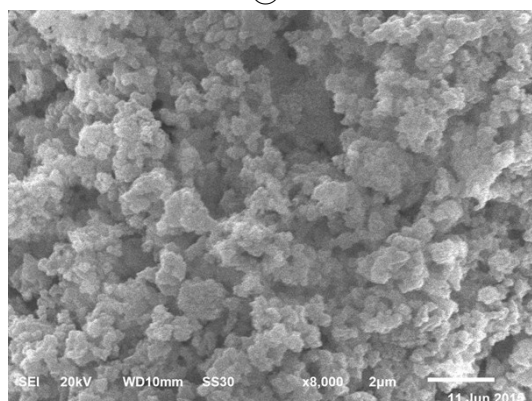
NH₂-MIL-101(Al)



S@M-1



S@M-2



S@M-3

Fig. S2a SEM images of S@M materials in comparison to the bulk NH₂-MIL-101(Al).

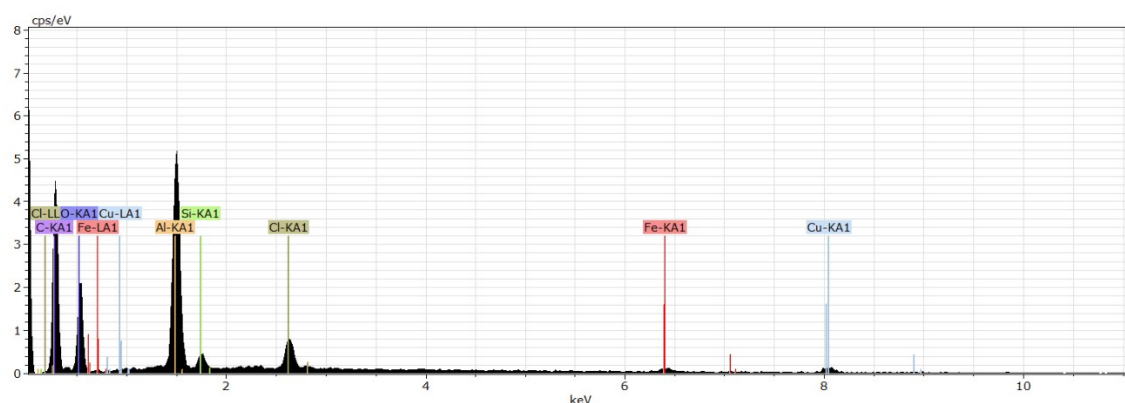


Fig. S2b Energy-dispersive X-ray spectrum of S@M-1 with peak assignment. Determination of the Al : Fe ratio was based on the Al-KA1 and the Fe-KA1 peaks (KA = $K\alpha$)

Temperature stability of S@M samples and thermogravimetric analysis of $[\text{Fe}(\text{HB}(\text{pz})_3)_2]$

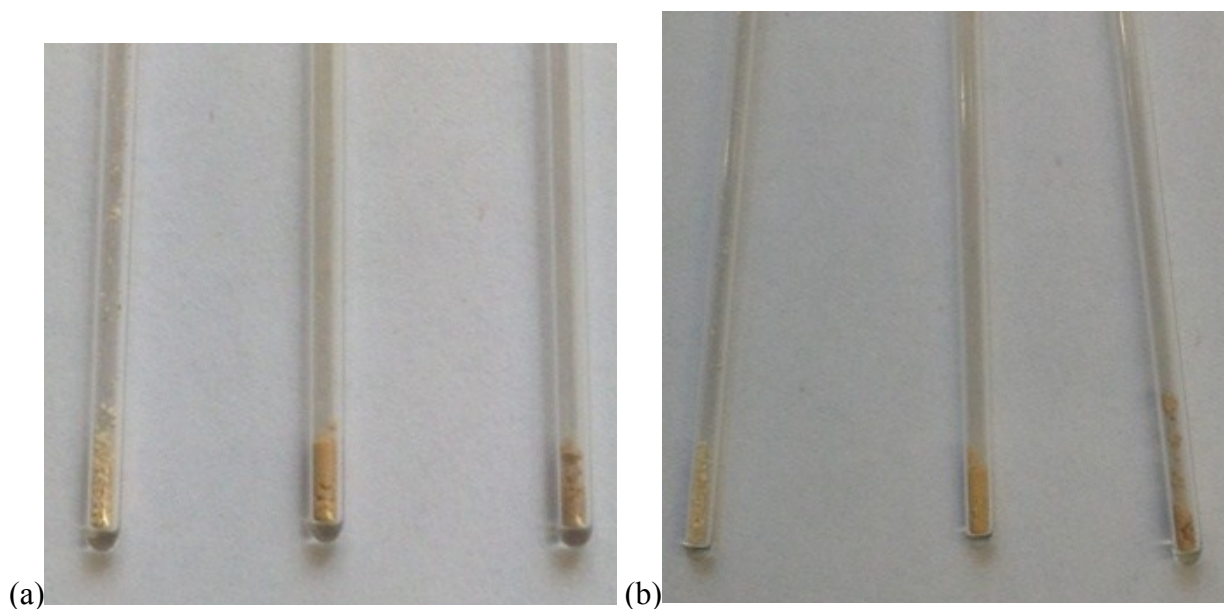


Fig. S3 Photographs of the S@M sample at 25 °C (a) and after heating to 230 °C (503 K) (b). The order from left to right is S@M-1, S@M-2 and S@M-3 for each photograph.

The photographs in Fig. S3b were taken after heating in a melting point determination device to 230 °C, with a heating rate of 10 °C/ min. After heating, all samples kept the same color, and the SCO still can be triggered by the addition of solvent; in this case, methanol was used.

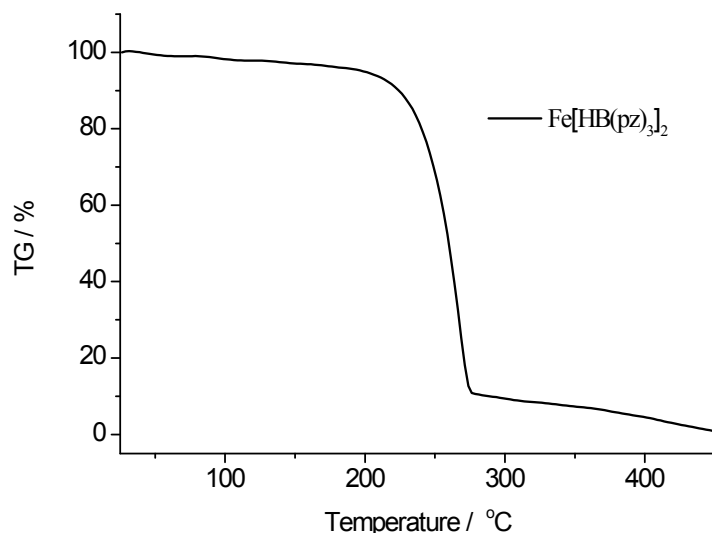


Fig. S4 TG curve for $[\text{Fe}(\text{HB}(\text{pz})_3)_2]$, which shows sublimation of the complex above 220 °C under nitrogen gas and ambient pressure.

Temperature dependent magnetism of $[\text{Fe}(\text{HB}(\text{pz})_3)_2]$ and the S@M materials

Introductory note. μ is magnetic moment per one Fe^{2+} ion given in Bohr magnetons (μ_B). For spin only value magnetic moment can be calculated as $\mu = g\sqrt{S(S+1)} \mu_B$, or experimentally from the $\mu = \sqrt{8\chi_{\text{mol}}T}$ relation. For 4 unpaired electrons, and for spin only magnetic moment, $\chi_{\text{mol}}T$ ought to be 3 emu K $\text{Oe}^{-1}\text{mol}^{-1}$. In low spin state, LS, $S = 0$, i.e. $\mu = 0$ and complex should be diamagnetic. In practice it is not so because of a number of factors. Among them the existing positive temperature independent paramagnetism of Fe(II) and the presence of species with non-zero spin, as $^5\text{T}_{2g}$ level (HS) is populated in some degree even at low temperatures, and because of Fe^{3+} admixtures.

In high spin state with 4 unpaired electrons $S = 2$ and $\mu = 4.9 \mu_B$ (it is assumed that $g = 2$, where g is the Lande factor). In the real world values are usually larger, because spin-orbit interaction contributes to some extent. For Fe(II) $L = 2$ and $S = 2$, and maximal magnetic moment can be about $5.48 \mu_B$. In the literature some authors claim that acceptable value for $\chi_{\text{mol}}T$ product, for Fe(II) complexes, is up to $3.92 \text{ emu K mol}^{-1} \text{ Oe}^{-1}$, i.e. $\mu = 5.6 \mu_B$.⁴

Literature data regarding $[\text{Fe}(\text{HB}(\text{pz})_3)_2]$ complex.

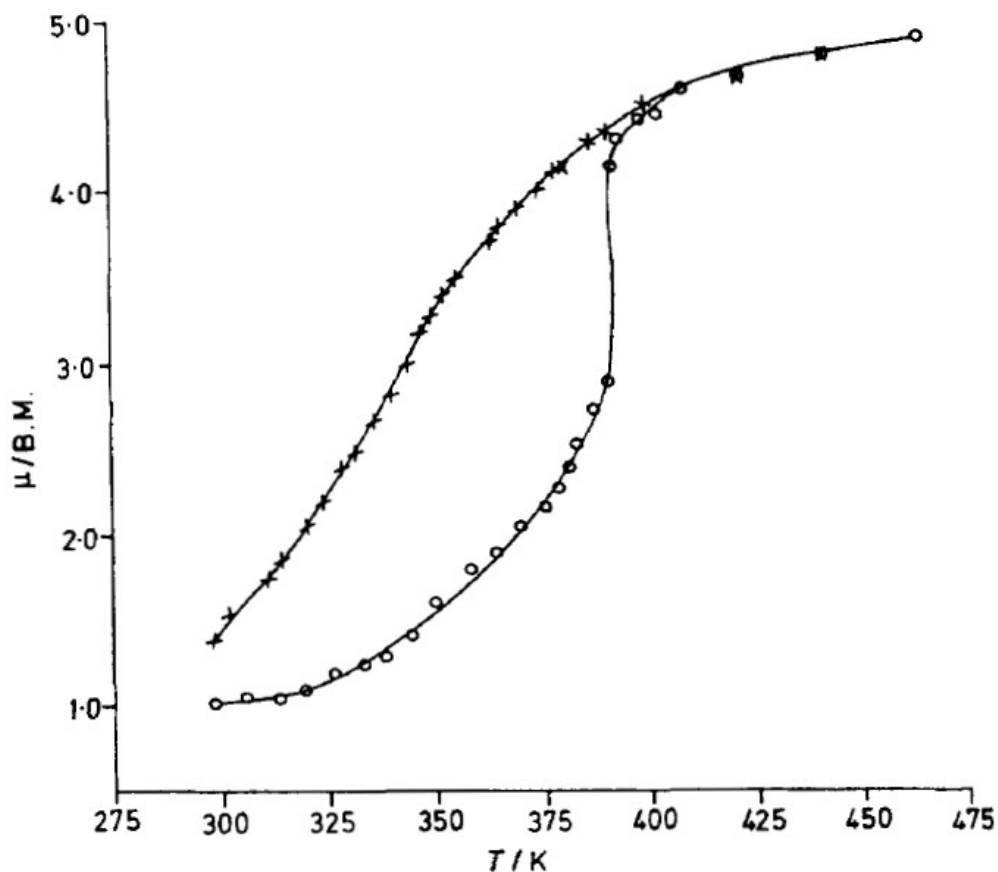


Fig. S5 Temperature dependence of the effective magnetic moment of crystalline $[\text{Fe}(\text{HB}(\text{pz})_3)_2]$ (open sphere for heating and cross for cooling). Figure taken from ref. 5.

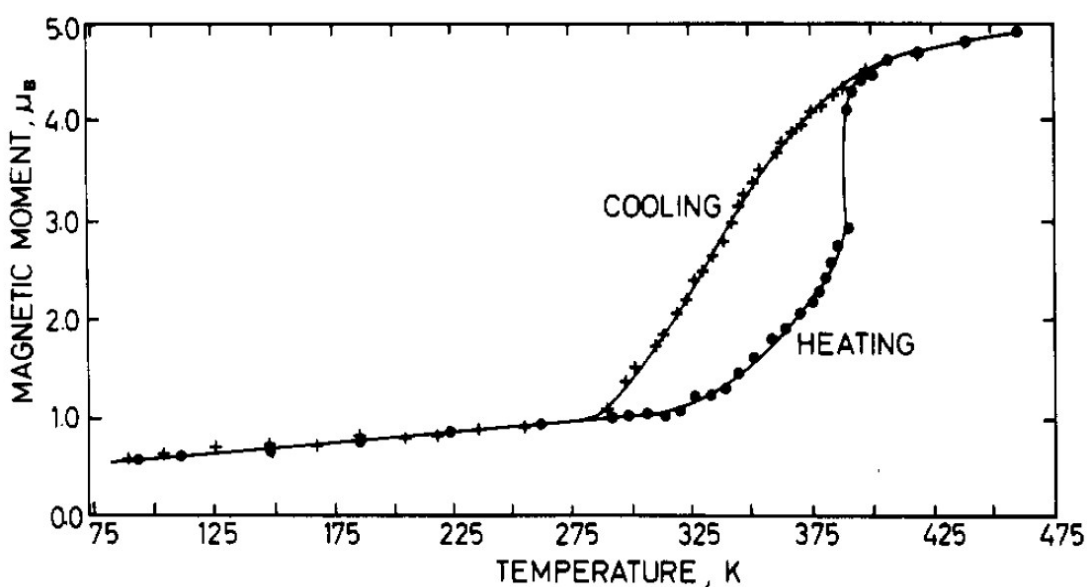


Fig. S6 Temperature dependence of the magnetic moment for $[\text{Fe}(\text{HB}(\text{pz})_3)_2]$ during heating and cooling. The figure is taken from ref.6

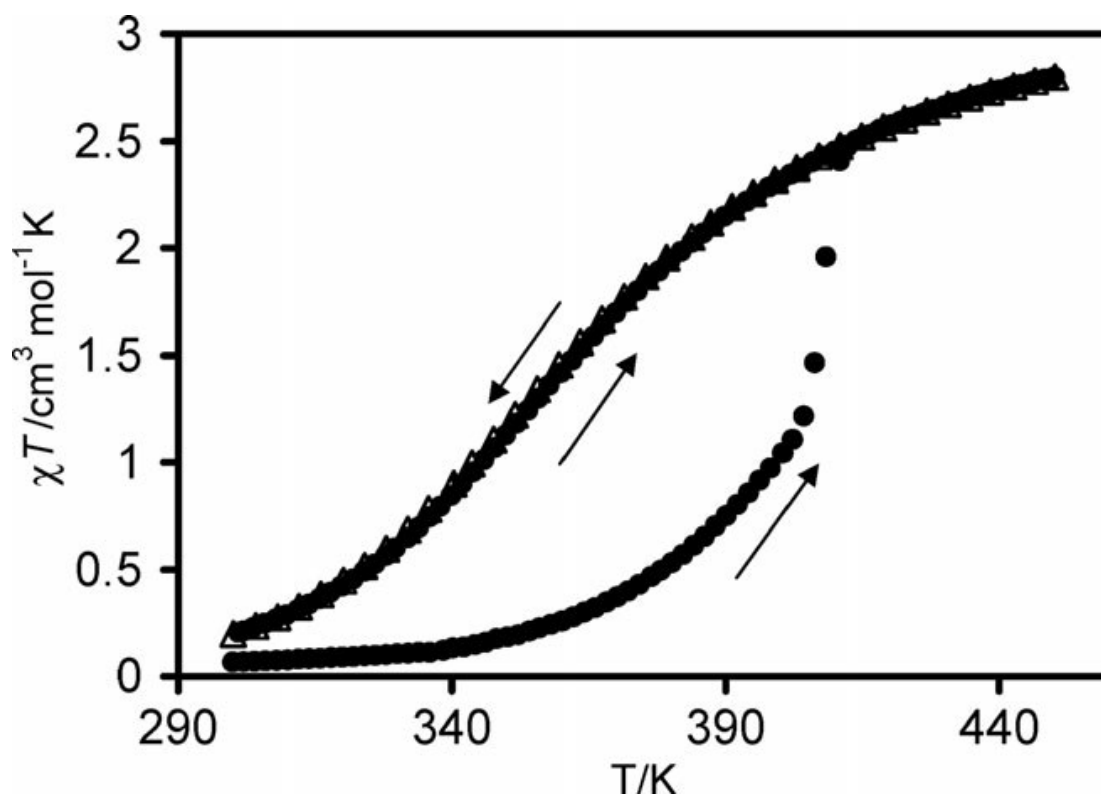


Fig. S7 The temperature dependence of the $\chi_M T$ product of $[\text{Fe}(\text{HB}(\text{pz})_3)_2]$ upon two successive thermal cycles (first cycle: closed circles, second cycle: open triangles). The figure is taken from ref. 1.

Experimental data on S@M composites. The molar susceptibilities were calculated as given below. Assuming that all the iron in the sample is incorporated in the form of $[\text{Fe}(\text{HB}(\text{pz})_3)_2]$, the relative content of the latter is calculated using the iron content determined by the AAS analytics. The content of actual content of the iron complex and the matrix in a sample with a weight m is $m \cdot x$ and $m \cdot (1-x)$, where x is the calculated content of the iron complex. The calculated weights allow to apply the diamagnetic corrections. In the case of the matrix it was determined experimentally for a non loaded sample to be $\chi_{\text{dia}} = -1.1 \cdot 10^{-9} \cdot T - 2.2 \cdot 10^{-7} \text{ emu g}^{-1} \text{ Oe}^{-1}$, while for the $[\text{Fe}(\text{HB}(\text{pz})_3)_2]$ the value of $-3.55 \cdot 10^{-4} \text{ emu g}^{-1} \text{ Oe}^{-1}$ estimated from the Pascal constants were used. The corrected absolute values of the susceptibilities, emu Oe^{-1} , are related to molar quantities, $v = m \cdot x / M_{\text{FeL2}}$, ($M_{\text{FeL2}} = 481.9$), thus giving the molar values, from which, subsequently the magnetic moment per one Fe-ion in Bohr magnetons is calculated using the $\mu = 2.828(\chi_{\text{mol}} \cdot T)^{0.5}$.

The spin-only value for one moles of iron ions is 4.9 Bohr magnetons, μ_B , but experimentally this value might be up to 5.6.

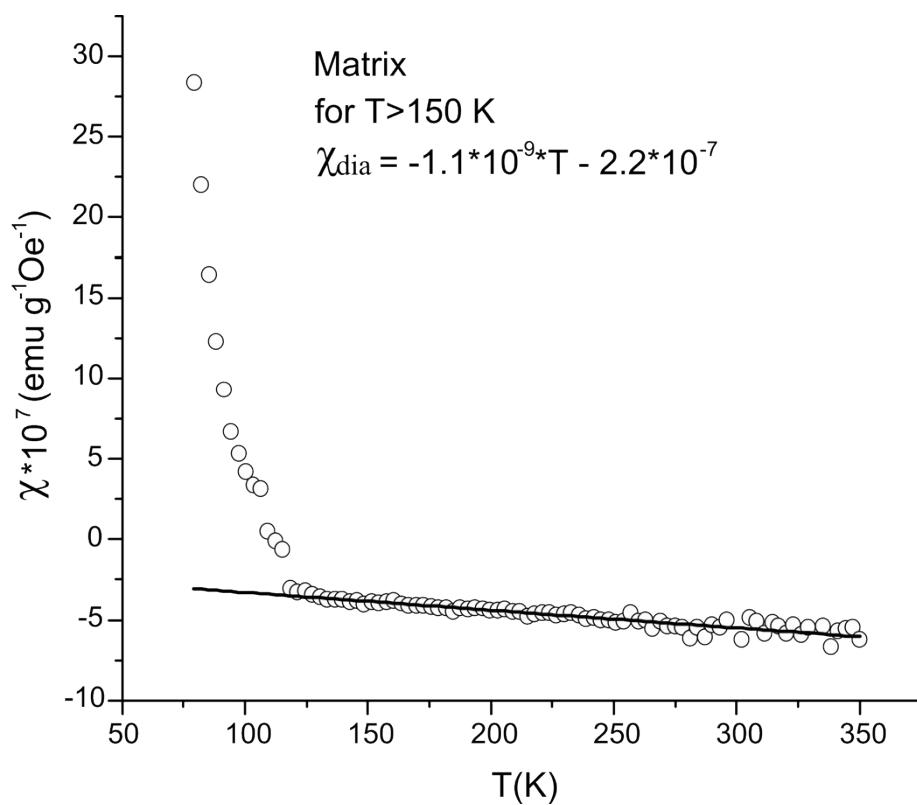


Fig S8 Temperature-variable magnetic curve for $\text{NH}_2\text{-MIL-101(Al)}$ reference sample.

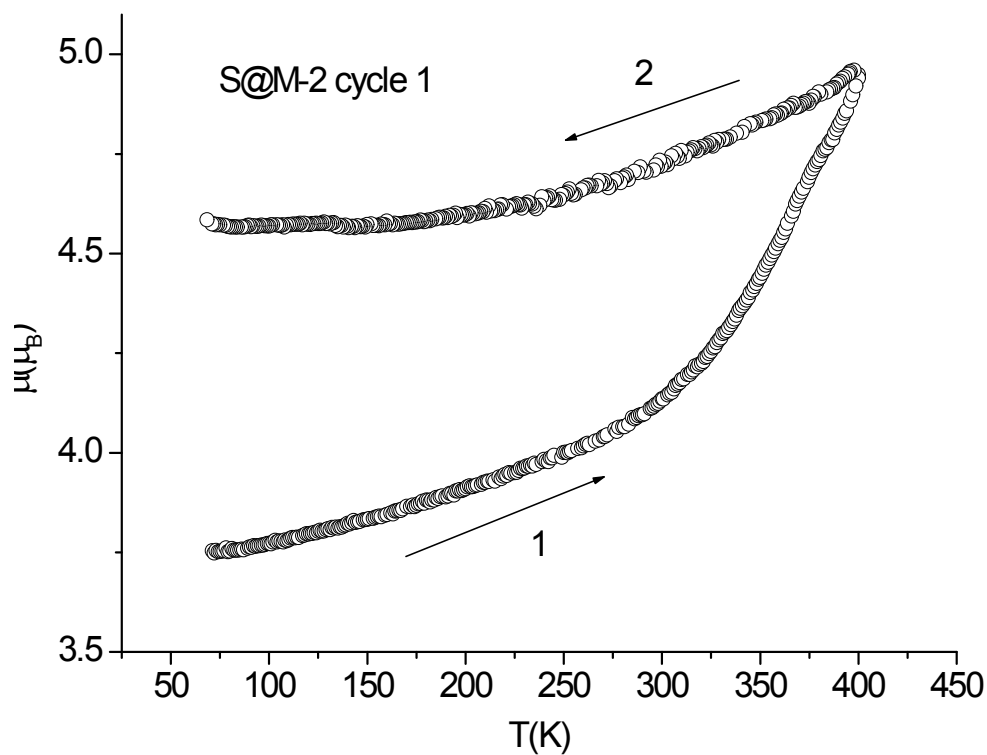


Fig S9 Temperature dependence of the magnetic moment for S@M-2 (first cycle).

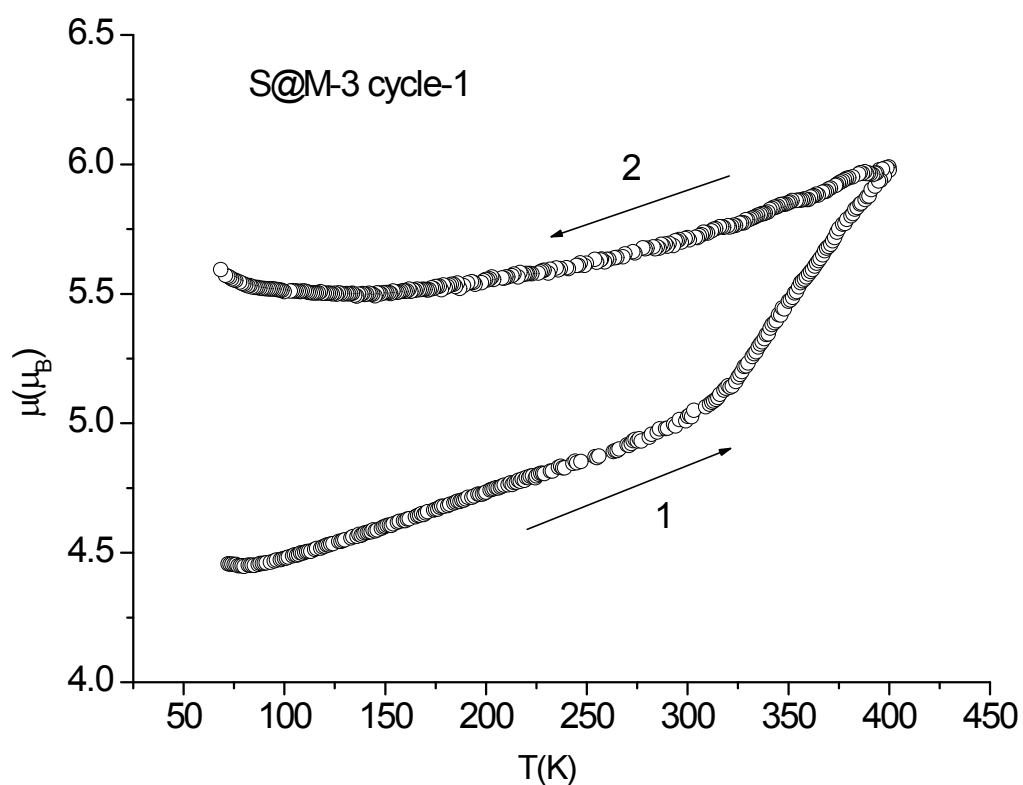


Fig S10 Temperature dependence of the magnetic moment for S@M-3 (first cycle).

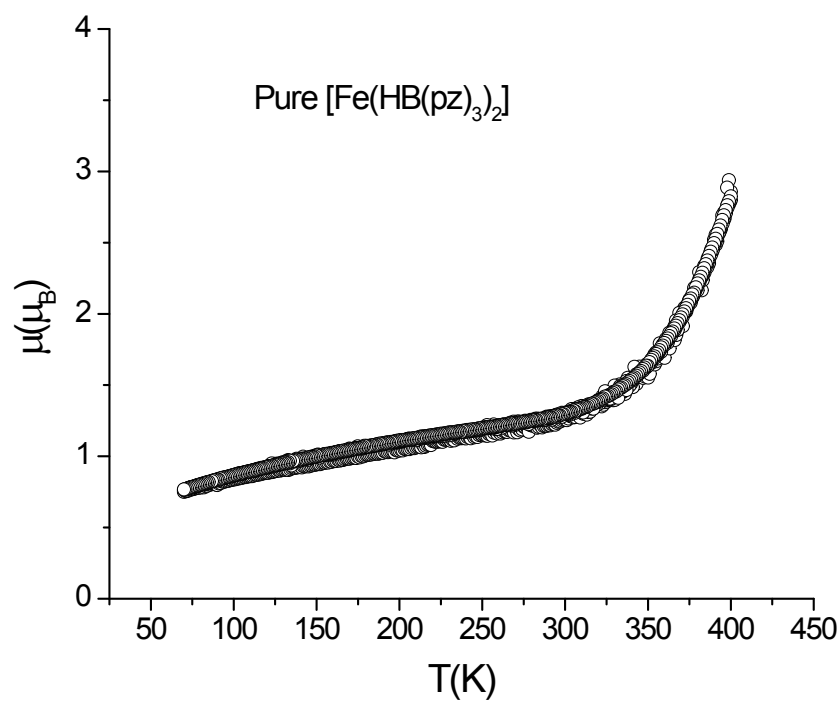


Fig S11 Temperature dependence of the magnetic moment for [Fe(HB(pz)₃)₂] (first cycle).

Temperature dependent diffuse reflectance spectrum of the S@M-3 material

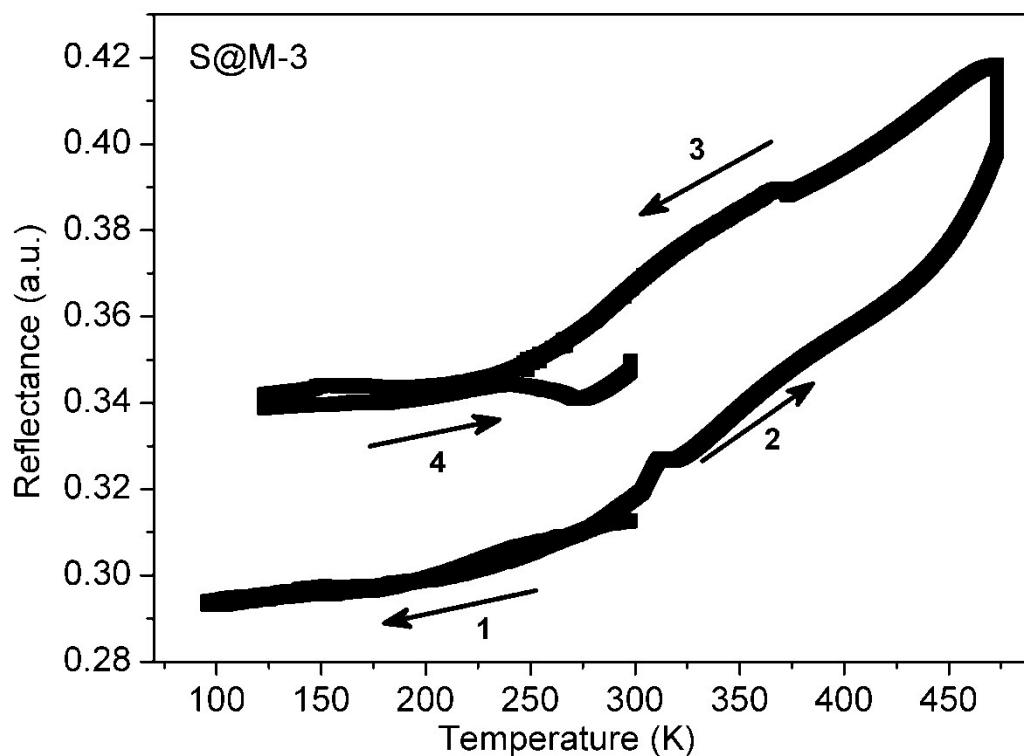


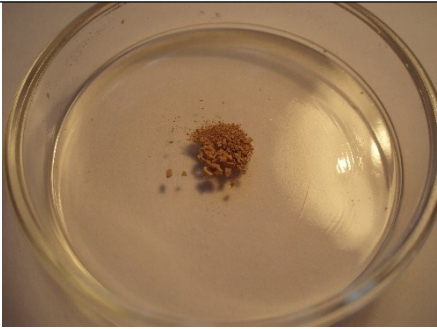

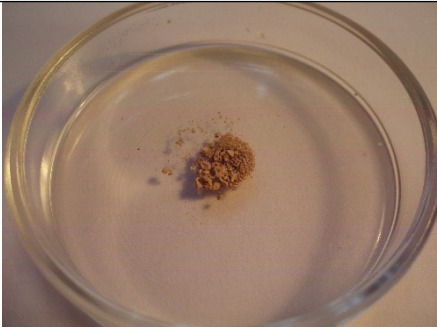
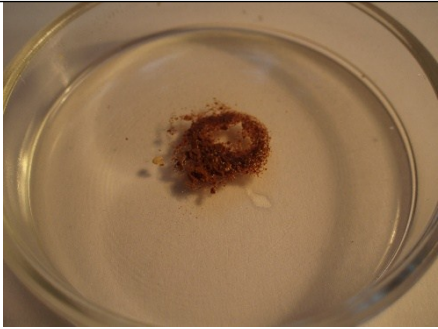
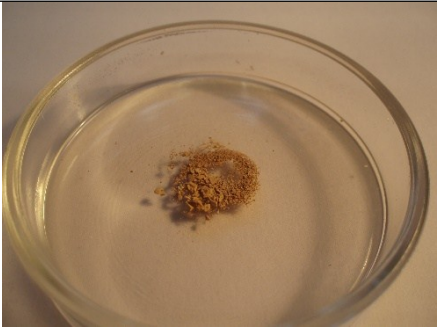



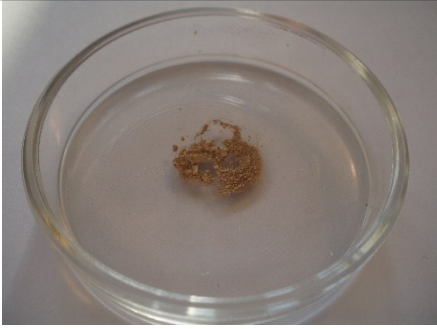



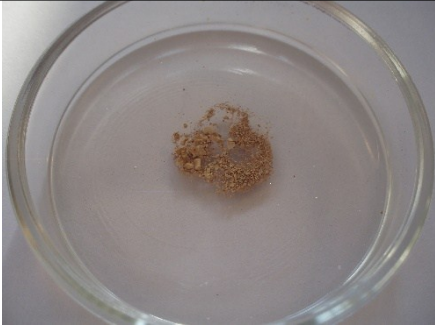

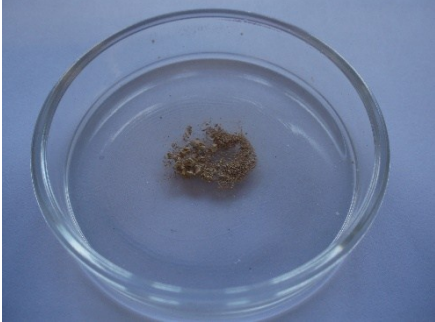







Fig. S12 Thermal dependence of the diffuse reflectance recorded on S@M-3 sample.

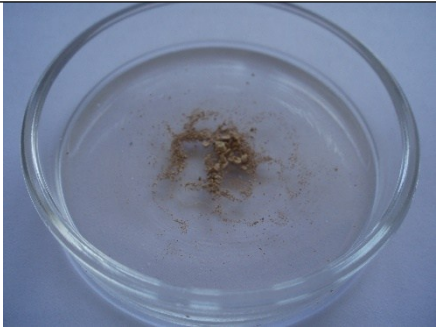
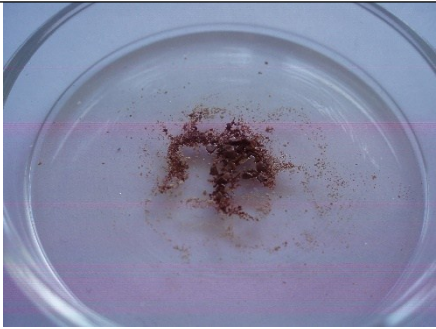

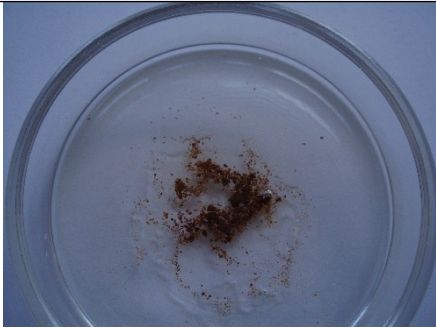



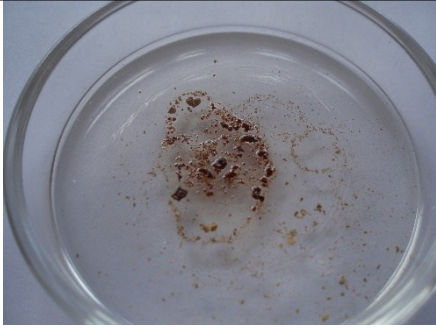

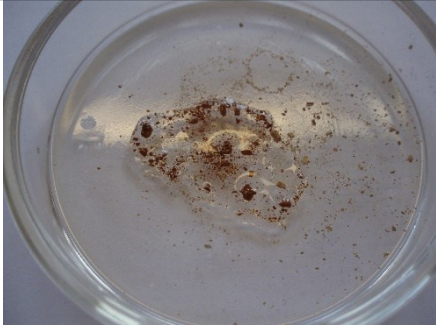
Table S1 Photographs of bulk $[\text{Fe}(\text{HB}(\text{pz})_3)_2]@\text{NH}_2\text{-MIL-101}(\text{Al})$ as sample S@M-2 with different solvents added for colour comparison.

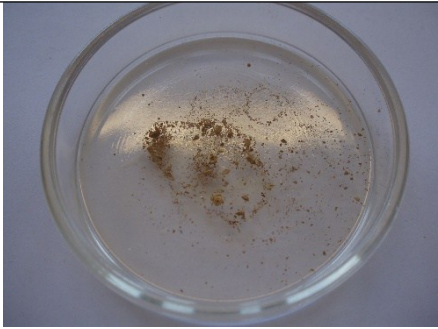

(The sample was dried after each new addition, either at 70 °C or at 120 °C, depending on the solvent's boiling point, under membrane pump vacuum (~ 10 Torr). The order in the following Table corresponds to the chronological order of solvent addition experiments.)

Solvent	before solvent addition	after solvent addition
CCl_4		

CHCl ₃		
CH ₂ Cl ₂		
CH ₃ CN		
THF		
MeOH		

i-PrOH		
n-BuOH		
n-pentane		
n-hexane		
n-heptane		

cyclohexane		
toluene		
H ₂ O		
mesitylene		
DMF		

ethylacetate		

- 1 L. Salmon, G. Molnár, S. Cobo, P. Oulié, M. Etienne, T. Mahfoud, P. Demont, A. Eguchi, H. Watanabe, K. Tanaka and A. Bousseksou, *New J. Chem.*, 2009, **33**, 1283–1289.
- 2 A. I. Kitaigorodskii, *Molecular Crystals and Molecules*, Academic Press, New York, 1973.
- 3 B. Seoane, C. Téllez, J. Coronas and C. Staudt, *Sep. Purif. Technol.*, 2013, **111**, 72–81.
- 4 A. S. Tolla, A. Banerjee, S. Stjepanovic, J. Li, W. W. Brennessel, R. Loloee and F. A. Chavez, *Eur. J. Inorg. Chem.*, 2013, 2115–2121.
- 5 B. Hutchinson, L. Daniels, E. Henderson, P. Neill, G. J. Long and L. W. Becker, *J. Chem. Soc., Chem. Commun.*, 1979, 1003–1004.
- 6 F. Grandjean, G. J. Long, B. B. Hutchinson, L. Ohlhausen, P. Neill and J. D. Holcomb, *Inorg. Chem.*, 1989, **28**, 4406–4414.